Thermochimica Acta 505 (2010) 14–21

Contents lists available at ScienceDirect

Thermochimica Acta

journal homepage: www.elsevier.com/locate/tca

Fast scanning power compensated differential scanning nano-calorimeter: 2. Heat capacity analysis

E. Zhuravlev, C. Schick*

University of Rostock, Institute of Physics, Wismarsche Str. 43-45, 18051 Rostock, Germany

ARTICLE INFO

Article history:
Received 18 January 2010
Received in revised form 18 March 2010
Accepted 22 March 2010
Available online 31 March 2010

Keywords:
Fast scanning nano calorimetry
DSC
Heat capacity
Differential power compensation
Crystallization
Polymer

ABSTRACT

Fast scanning calorimetry is an attractive tool to study kinetics and thermodynamics of materials created or used far from thermodynamic equilibrium. In the first part of this paper we describe a differential fast scanning nano-calorimeter utilizing a new power compensation scheme. The device is suitable for calorimetric experiments at controlled cooling and heating rates between 1 and 100,000 K/s. This part of the paper focuses on determination of specific heat capacity out of the measured data. Assuming time independent heat losses for sample and reference sensors at heating and cooling makes possible a heat capacity analysis based on symmetry arguments. The described procedure is not limited to chip-based fast scanning devices but can be applied to common DSC too. Due to the differential scheme and power compensation heat capacity of polymer samples with sample mass of a few 10 ng is available. Reproducibility of heat capacity is in the order of ±2% at optimum scanning rates. Uncertainty of specific heat capacity strongly depends on sample mass determination and is in the order of ±10%. Adding a small particle of a temperature calibration standard, e.g. indium or tin, on top of the polymer sample reduces uncertainty of temperature to about ±4 K.

1. Introduction

In polymers, pharmaceuticals, and metal alloys metastability is the rule rather than the exception, and the study of the kinetics of such systems has become an important issue [1,2]. For a thorough understanding of the kinetics of all kinds of temperature- and time-dependent processes related to metastability there is an urgent need for new (calorimetric) techniques enabling the use of high cooling and heating rates [3].

Conventional DSC is one of the few techniques that have already a relatively large dynamic range of scanning rates. They allow (quasi) isothermal measurements and scanning rates up to 10 K/s for power compensated DSCs [1,4]. Several approaches are known how to overcome these limitations. Most of them are based on thin film techniques. Quasi-adiabatic scanning calorimetry at high heating rates, ca. 500 K/s, was developed by Hager [5] and even for rates up to 10^7 K/s, by Allen and co-workers [6,7] and others [8,9]. Heat capacity determination in these quasi-adiabatic calorimeters is relatively simple because heat losses can be neglected in first approximation. Nevertheless, a more quantitative analysis requires quite some corrections also for these calorimeters [7–12]. But as mentioned above, further investigation of metastable phase formation can be obtained only if the same high controlled cooling rates are available too. Therefore a single sensor non-adiabatic fast scanning calorimeter [13–16] was developed.

The main problem for heat capacity determination for the non-adiabatic single sensor device is the subtraction of the heat loss function. It is realized as a subtraction of a 3rd to 5th order polynomial function [16]. But as soon as several sharp events in the sample occur, the error in determination of the loss polynomial increases dramatically (Fig. 1).

A differential power compensated fast scanning calorimeter was set up to overcome these problems at least in part. It covers the scanning rate range between 1 and 10^5 K/s in heating and cooling. The device, as described in the first part of this paper [17], uses the same low addenda heat capacity sensors [18] as previously used for the single sensor device [14,16,19]. The presence of an empty reference sensor reduces the influence of heat losses and addenda heat capacity on the obtained data. For a better sample temperature control, particularly in the transition regions, a power compensation was introduced, this way following the work by Rodriguez-Viejo and co-workers [20]. To improve signal to noise ratio and resolution of the device, even under fast scanning conditions, an analog power compensation technique was implemented. A differential power compensation scheme provides, under conditions of ideal symmetry of both sensors, directly the heat flow rate into the sample, which simplifies heat capacity calculation. Furthermore, user-friendly experiment management software and a software package for data evaluation were developed.

* Corresponding author. Tel.: +49 381 498 6880; fax: +49 381 498 6882.
E-mail address: christoph.schick@uni-rostock.de (C. Schick).

0040-6031/$ – see front matter © 2010 Elsevier B.V. All rights reserved.
doi:10.1016/j.tca.2010.03.020

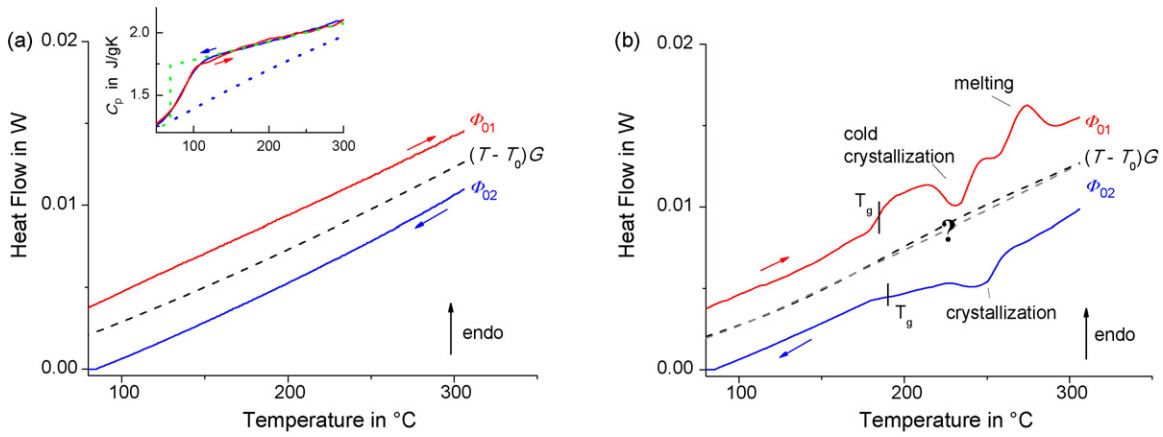

Fig. 1. (a) Heat flow rate at heating Φ_{01} and cooling Φ_{02} for a heating–cooling scan at 2000 K/s for ca. 480 ng poly (ethylene terephthalate) (PET) sample [15]. The heat loss curve $(T - T_0)G$ is determined outside the transition regions as the symmetry line between Φ_{01} and Φ_{02}. (b) Problems of heat loss determination in case of complex overlapping events in the sample during heating and cooling.

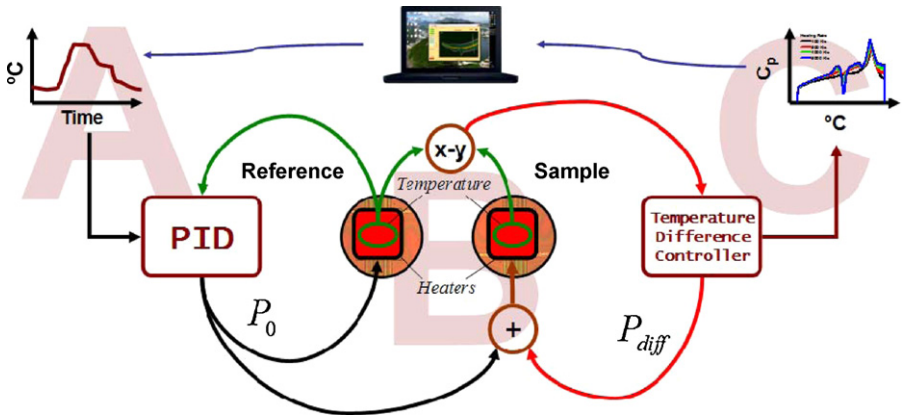

Fig. 2. Scheme of the power compensated fast scanning calorimeter. A, the time-temperature profile is generated by the user and is provided to the PID controller through a DAC board. B, sample temperature is made to follow precisely the required profile by means of control loop. C, the resulting temperature difference can be recalculated to heat flow rate and sample heat capacity as shown below.

The developed new power compensation scheme realizes such separate control loops as shown in part 1 [17,21]. It was already successfully applied to the study of polymers [22–25] and metals [26–28]. Compared to the PerkinElmer power compensation scheme [29] the new scheme allows a more precise control of the temperature of both sensors. But the proportionality between the remaining temperature difference in the differential control loop and the differential heat flow rate is lost. Therefore the new scheme requires the measurement of more than only one signal to allow recalculation of the power difference as it is described in part 1 [17].

The practical realization of the control scheme described in Ref. [17] is shown in Fig. 2. The user defined time-temperature profile is recalculated into a voltage and provided as the setpoint for the PID controller. The PID controller makes the temperature of the reference sensor to follow the profile by adjusting power P_0 to its heater. The same power P_0 is applied to the sample loaded sensor. The difference between the temperatures of reference and sample side is minimized by the differential controller by adding power P_{diff} to the sample side. The actual realization of this scheme using thin film chip calorimeter sensors is shown in Fig. 2.

The resistive film-heaters of the sensors provide the power, which is supplied to the membrane/sample interface and propagates through the sample, membrane and the ambient gas. For a perfectly power compensated system power is distributed in a way that both sensors are always at the same temperature, T, and scanned at the programmed rate, dT/dt, independent of any heat effect in the sample. Assuming an ideally symmetric differential system, which means equal addenda heat capacities C_0 on both sides and equal heat losses $P_{loss}(T)$ to the surrounding on both sides, the heat balance equations for both sensors are as follows:

$$\text{reference}: \quad C_0(T)\frac{dT}{dt} = P_0(T) - P_{loss}(T) \tag{1.1}$$

$$\text{sample}: \quad (C_0(T) + C(T))\frac{dT}{dt} = P_0(T) + P_{diff}(T) - P_{loss}(T) \tag{1.2}$$

where C is sample heat capacity. In this particular case the difference between Eqs. (1.2) and (1.1) yields:

$$C(T)\frac{dT}{dt} = P_{diff}(T) \tag{1.3}$$

where P_{diff} is the difference between the power supplied to the sample and the reference sensors.[1] Consequently, the aim was to set up a system with near to perfect power compensation, which allows determination of $P_{diff}(T)$ and finally to correct for unavoidable asymmetries between both sides in real measurements at high scanning rates. The hardware was designed for that aim having in mind anticipated scanning rates of up to 100,000 K/s [17].

[1] These considerations also hold for conventional DSCs and therefore the procedure described below can be applied to conventional DSC too.

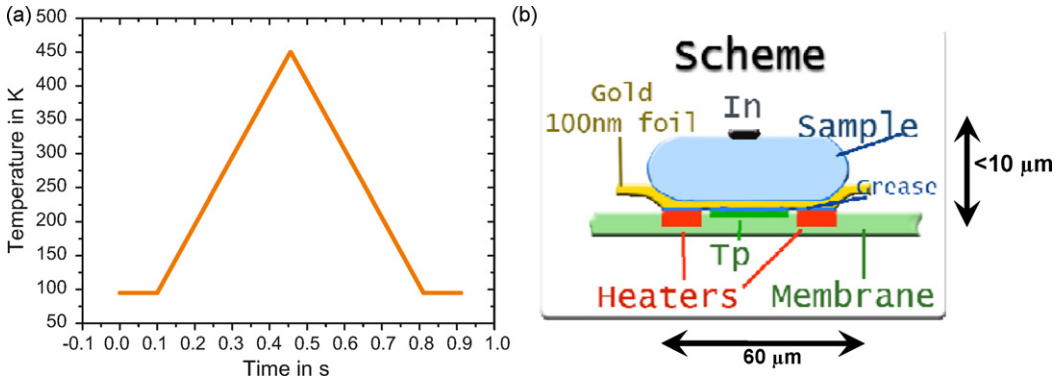

Fig. 3. Typical measurement temperature profile (a) and sample preparation scheme (b).

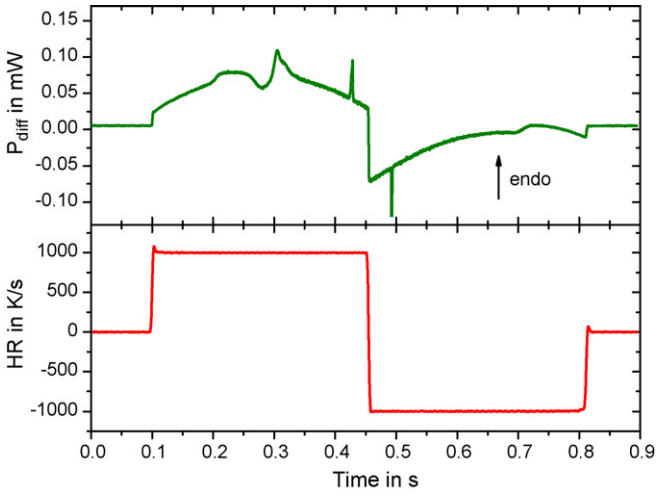

Fig. 4. Reference heating rate (bottom) and differential heat flow (power) (top) during the scan at 1000 K/s for a PCL sample of 50 ng with a small indium particle on top.

2. Experimental

The device is intended to measure nanogram samples on controlled cooling and heating at high rates. A typical temperature profile, consisting of isotherms, heating and cooling, is shown in Fig. 3. The sample is placed in the center of the membrane covering the heated area. To homogenize temperature laterally a 100 nm thick gold foil is used. Silicon oil is placed in between the gold sheet and the membrane making a good wet thermal contact. Only a small amount of oil, not adding much to addenda heat capacity, stays there due to capillary forces. A similar foil is placed in the same way on the reference sensor. The foil itself (70 µm × 70 µm × 100 nm thick) adds negligibly small addenda heat capacity in comparison with 10 µm thick polymer and the difference between two similar foils is even smaller, ca. 0.5 nJ/K. A small piece of the material under investigation is placed on the gold foil on the sample sensor. After first melting it spreads over the foil and creates a good thermal contact with the foil. The dimensions of the prepared sample should not exceed the size of the heated area and, depending on maximum rate, 10 µm in height to avoid temperature gradients inside the sample [15]. To ensure the correct sample temperature measurement and for demonstration purposes a small indium particle was placed on top of the sample.

The temperature profile in Fig. 3 consists of an isotherm for 0.1 s at 100 K, 1000 K/s heating from 100 to 450 K and successive cooling at the same rate back to 100 K followed by another 0.1 s isotherm. Poly(ε-caprolactone) (PCL) was used as sample. It has a glass transition temperature of ca. 200 K and melts at about 330 K. Indium has a rate independent melting point T_m = 229.8 K and shows supercooling of a few Kelvin only.

The result of the experiment is the differential heat flow as shown in Fig. 4, which includes the heat flow to the sample but also temperature dependent differential heat losses ($P_{loss}^{diff}(T)$).

The bottom curve in Fig. 4 shows the result of digital differentiation of the measured sample temperature. It shows the well-controlled constant heating rate with short (3 ms) overshoots at the beginning and end of heating and cooling.

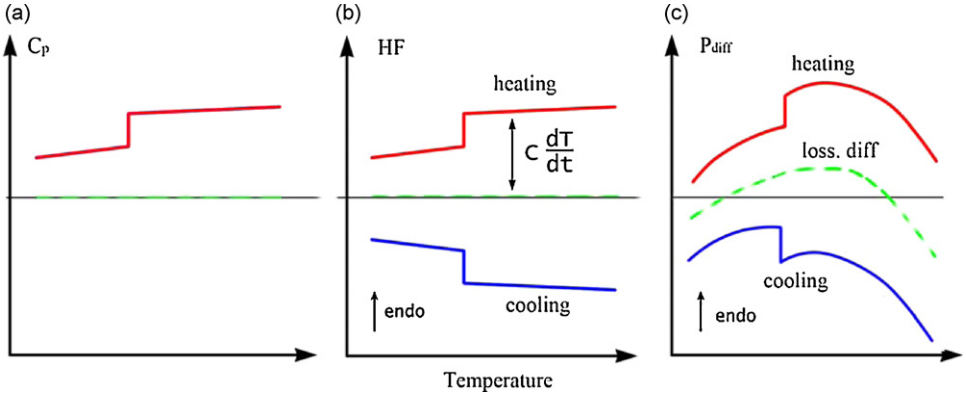

Fig. 5. Origins of the measured signal. (a) Temperature dependent heat capacity including a step at T_g. (b) On heating or cooling at the same rate a positive or negative heat flow into or out of the sample is required. (c) The heat loss difference (dashed green line) is added to the heat flows from (b). This sum is the finally measured power difference. (For interpretation of the references to color in this figure legend, the reader is referred to the web version of the article.)

3. Heat capacity calculation

3.1. Heat balance

Scanning calorimeters determine the power difference between reference and sample side during controlled temperature treatment [17,30]. The heat capacity of the sample during the scan can be recalculated from P_{diff} and heating rate using the heat balance Eqs. (1.1)–(1.3), or more precisely:

$$\text{reference}: \quad C_0^{\mathrm{ref}} \frac{\mathrm{d}T^{\mathrm{ref}}}{\mathrm{d}t} = P_0^{\mathrm{ref}} - P_{\mathrm{loss}}^{\mathrm{ref}}(T) \tag{1.4}$$

$$\text{sample}: \quad (C_0^{\mathrm{sample}} + C_{\mathrm{sample}}) \frac{\mathrm{d}T^{\mathrm{sample}}}{\mathrm{d}t} = P_0^{\mathrm{sample}} + P_{\mathrm{diff}} - P_{\mathrm{loss}}^{\mathrm{sample}}(T) \tag{1.5}$$

where P_0 and P_{diff} are average and differential power generated by the heaters, C_0 and C_{sample} are heat capacity of empty sensor (addenda) and sample, respectively. $\mathrm{d}T/\mathrm{d}t$ is temperature scanning rate and $P_{\mathrm{loss}}(T)$ is heat loss to the surrounding. Superscripts *sample* and *ref* denotes sample and reference sensors, respectively.

The addenda heat capacity of the heated part of the membrane is ca. 30 nJ/K at room temperature. Using sensors from the same wafer the difference in addenda heat capacity is of the order of 0.6 nJ/K (see inset in Fig. 7(b) below). Therefore we can neglect the difference between reference and sample side addenda heat capacities compared to sample heat capacity of commonly more than 10 nJ/K and express sample heat capacity as:

$$C_{\mathrm{sample}} \frac{\mathrm{d}T}{\mathrm{d}t} = P_{\mathrm{diff}} - P_{\mathrm{loss}}^{\mathrm{diff}}(T), \tag{1.6}$$

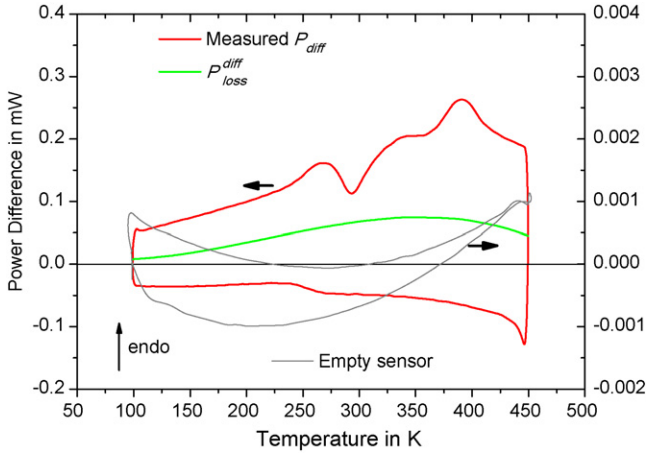

Fig. 6. Power difference (red curve) on heating and cooling used for determination of heat loss difference $P_{\mathrm{loss}}^{\mathrm{diff}}(T)$ (green center curve). iPP sample of ca. 56 ng at 1000 K/s scanning rate. The light grey curve shows the power difference from an empty sensor at a 100-fold enlarged scale (right axis). (For interpretation of the references to color in this figure legend, the reader is referred to the web version of the article.)

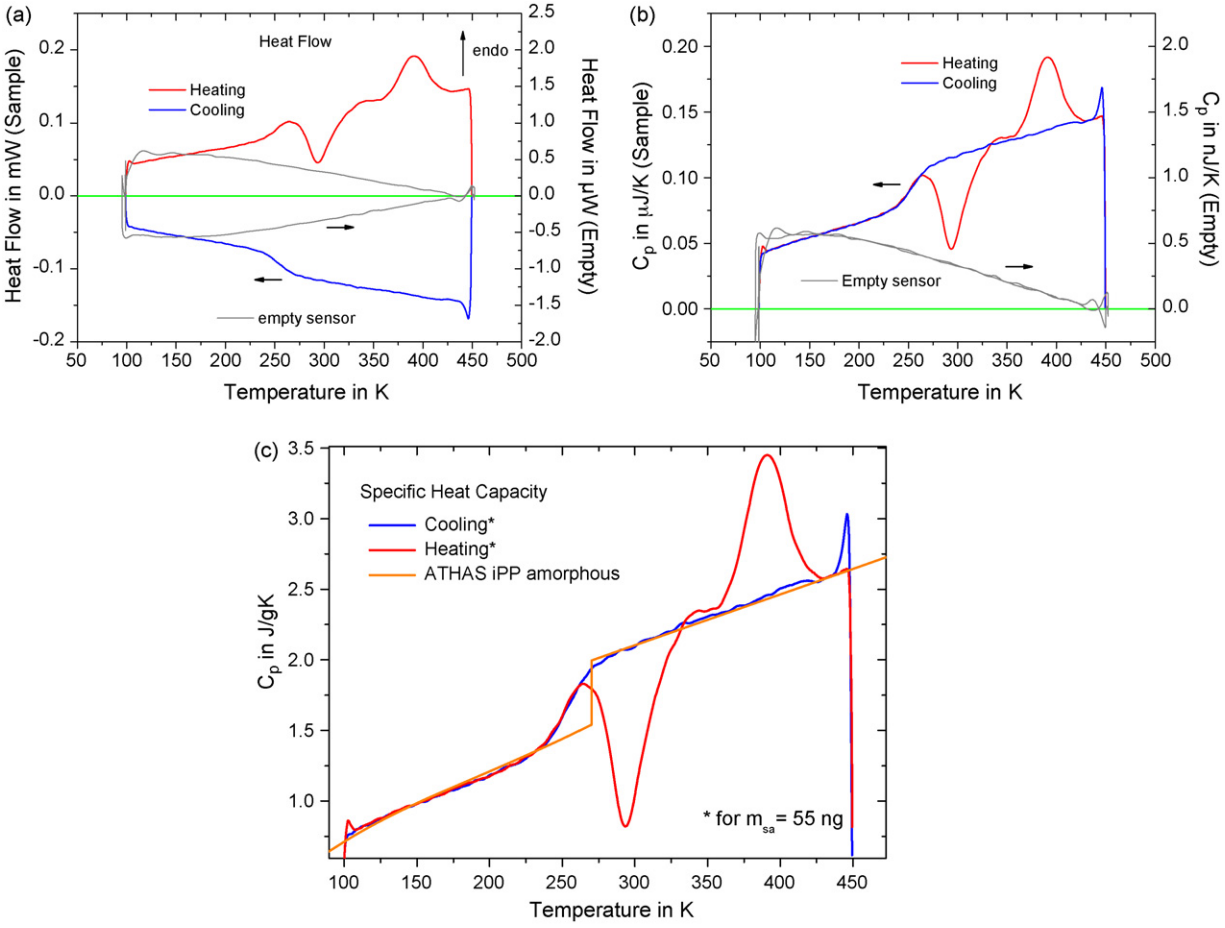

Fig. 7. iPP sample of ca. 56 ng at 1000 K/s scanning rate. (a) Heat flow rate to the sample (red and blue curves, left axis) and from the empty sensor (light grey curve, right axis 100-fold magnified) recalculated by subtracting the power difference shown in Fig. 6 from the measured data. (b) Sample heat capacity (red and blue curves, left axis) and addenda heat capacity difference from the empty sensors (light grey curve, right axis 100-fold magnified). (c) Specific heat capacity curve determined using liquid specific heat capacity above melting at 430 K from ATHAS databank [31]. (For interpretation of the references to color in this figure legend, the reader is referred to the web version of the article.)

Determination of P_{diff} for a fast scanning calorimeter is described in Ref. [17]. The differential loss function $P_{loss}^{diff}(T)$ is a smooth function of temperature containing asymmetries of the system including the difference in heat losses and P_{asym}, containing all other differences between the two sensors. The latter can be modified by hardware adjustments to minimize $P_{loss}^{diff}(T)$ and therefore the difference between P_{diff} and $C_{sample}(dT/dt)$. The influence of the heat loss difference on heat capacity determination and its correction is described next.

3.2. Determination of differential loss function

The measured quantity by differential scanning calorimeters is the power difference between sample and reference sensor. To better understand interpretation of the obtained data we consider once again the different causes of the obtained signals (Fig. 5). As an example a polymer sample was chosen because of its good adhesion properties and well-defined thermal contact properties. The sample heat capacity shows solid and liquid heat capacity below and above the glass transition (Fig. 5(a)). When the sample is heated it requires a heat flow into it and the same heat flow out of it on cooling at the same rate (Fig. 5(b)). Nevertheless, the measured power difference is the heat flow to the sample plus the smooth temperature dependent curve representing all asymmetries of the differential system (Fig. 5(c)). This is a schematic representation of $P_{loss}^{diff}(T)$ from Eq. (1.6). As shown by Minakov and Schick [14] the chip sensors utilized for fast scanning calorimetry behave quasi-static up to rates of 10^5 K/s. Only at higher rates time dependence of addenda heat capacity (heated area of the membrane) and heat losses have to be considered. The same can be considered for common DSCs. Therefore the same differential loss curve is added to the heat flow signal originating from the heat capacity (Fig. 5(b)), independent on heating rate or thermal history of the sample. Then the differential loss curve can be determined under optimal experimental conditions, e.g. if only a glass transition and no crystallization and melting occurs. This differential loss curve is then applicable for the correction of all other measurements for this particular sample as shown below.

If we are interested in sample heat capacity it requires correction of the measured data in the reverse order. The first step, determination of the heat loss difference line in the whole temperature range of interest is the main task for determining sample heat capacity. In contrast to power compensated DSC it is not possible to determine this line experimentally from an empty measurement [22,30]. Similar to heat flux DSCs the loss function of the chip-based sensors depends on the sample under investigation. If, for example, a 50 μm diameter spherical metal sample is measured the heat exchanging surface is nearly doubled compared to the flat reference sensor [27]. Under such conditions the assumption of symmetry between both sensors is seriously violated and yields strong curvature and slope of the $P_{loss}^{diff}(T)$ symmetry line between heating and cooling as shown in Figs. 5 and 6. Furthermore, transitions on heating and cooling may occur at different temperatures and have different width. Then the symmetry line does not equal the average between both curves in the whole temperature range but only outside the transitions. In Fig. 6 these transitions are glass transition, cold crystallization, and melting of isotactic polypropylene (iPP) on heating and only glass transition on cooling. The construction of the loss curve $P_{loss}^{diff}(T)$ therefore requires inter- or extrapolation into the transition region from outside the transitions as shown in Fig. 6. Because it is not a simple task to find an analytical expression for $P_{loss}^{diff}(T)$ for each sample under investigation it is recommended to search for a curve, as smooth as possible, describing $P_{loss}^{diff}(T)$ and yielding equal heat capacity outside the transition regions, where heat capacity is sample history and time independent. For polymers these regions are commonly below glass transition and above melting temperature, as shown below.

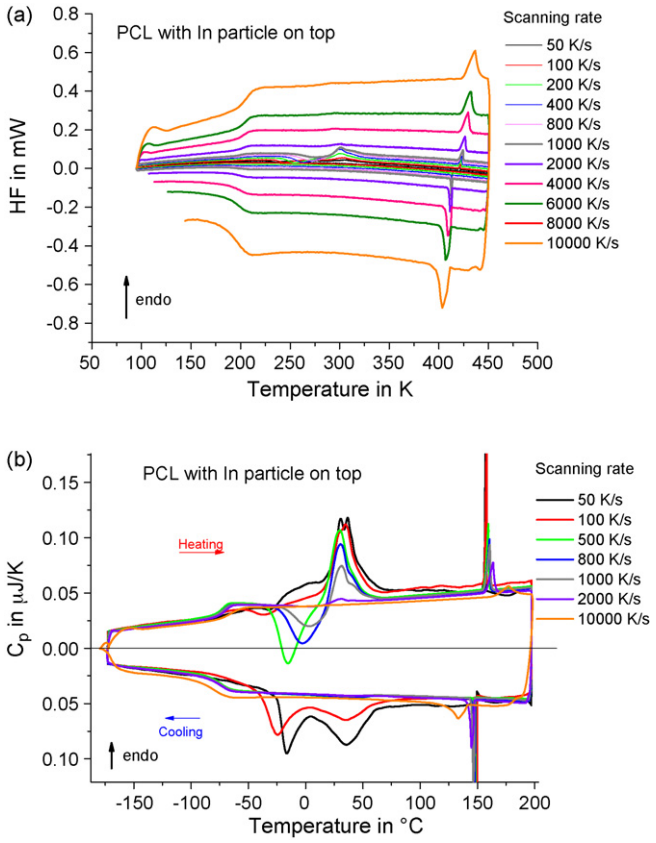

Fig. 8. Cooling–heating–cooling scans of a PCL sample at different rates. (a) Power difference measured and (b) heat capacity recalculated using one common curve for heat loss correction. $P_{loss}^{diff}(T)$ was determined from the measurement at 1000 K/s.

In the differential fast scanning calorimeter measurements $P_{loss}^{diff}(T)$ can be approximated with a smooth 2nd or 3rd order polynomial. This fact and the significant reduction of $P_{loss}^{diff}(T)$ to a value comparable to the heat capacity contribution to the heat flow are the main advantages of the new device in comparison to the single sensor technique where a 3rd to 5th order polynomial is used to describe the steeply increasing loss curve (see Fig. 1). The final calculation of heat flow difference to sample heat capacity is shown in Fig. 7. First, the $P_{loss}^{diff}(T)$ curve (green center curve in Fig. 6) is subtracted from the measured data. The result is shown in Fig. 7(a). Dividing curves for heating and cooling by the respective scanning rates yields heat capacity as function of temperature as given in Fig. 7(b).

The direct mass determination of the micron-sized samples is a complex task, which is better to avoid. To calculate specific heat capacity out of the data in Fig. 7(b) one has to estimate sample mass indirectly. One possibility is to use reference specific heat capacity data for the particular material from literature or independent measurements. For most polymers specific heat capacity data can be found in ATHAS databank [32]. Knowing specific heat capacity at a temperature T^* away from phase transitions, e.g. in the melt, one can estimate sample mass by comparing measured heat capacity with the known specific heat capacity ($m_{sample} = C_{sample}(T^*)/c_{ATHAS}(T^*)$) [12]. The resulting specific heat capacity for heating and cooling of iPP by comparing with ATHAS data for liquid heat capacity at 430 K is shown in Fig. 7(c). For sample mass (56 ± 5 ng) good agreement between measured heat capacity

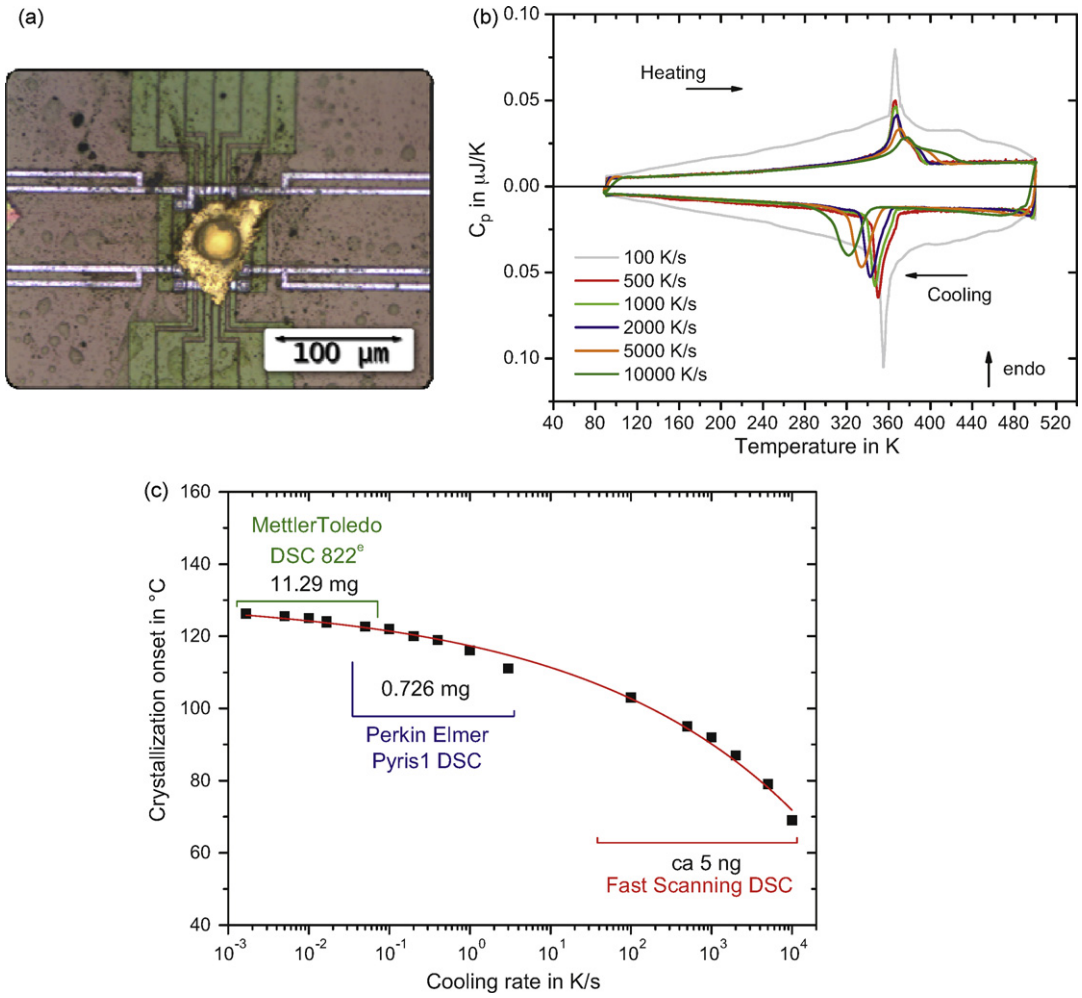

Fig. 9. (a) Sample preparation on sensor XI-320 with a gold foil under the UHMWPE sample. (b) Crystallization and melting of UHMWPE at different cooling and heating rates. (c) Peak onset temperature for nonisothermal crystallization in a wide range of cooling rates achieved by combining three calorimeters. The line is a guide for the eyes.

and expected specific heat capacity in the whole temperature range of the measurement is achieved.

To demonstrate that $P_{\text{loss}}^{\text{diff}}(T)$ depends only on temperature and not on scanning rate (time) a PCL sample was scanned at different rates from 100 to 10,000 K/s. The resulting differential power curves are shown in Fig. 8. Each curve consists of cooling and heating scans at the same rate.

As seen from Fig. 8(a) all curves are symmetric around one line, which corresponds to $P_{\text{loss}}^{\text{diff}}(T)$. For measurements in a wide range of scanning rates or other thermal histories it is therefore preferable to determine $P_{\text{loss}}^{\text{diff}}(T)$ under optimal conditions, e.g. at a rate where only the glass transition is seen and not crystallization and melting. Then the $P_{\text{loss}}^{\text{diff}}(T)$ curve can be determined with high confidence and applied for all other curves as long as the sample does not change position, shape or color (changing losses). From Eq. (1.6) it follows that at zero or close to zero heating rate the left side of the equation becomes zero and $P_{\text{loss}}^{\text{diff}}(T)$ equals $P_{\text{diff}}(T)$, allowing a simple determination of $P_{\text{loss}}^{\text{diff}}(T)$. Unfortunately, this procedure does not work because at very low rates the sample commonly starts to flow and the chip may be heated as a whole, including the cold junction of the thermopile. As soon as the $P_{\text{loss}}^{\text{diff}}(T)$ curve is determined, the differential power can be recalculated into heat capacity according to Eq. (1.6). For selected rates heat capacity is shown in Fig. 8(b). The scatter of the data at 450 K is about ±5 nJ/K. This corresponds to a scatter of ±8% for scanning rates between 50 and 10^4 K/s, with the largest uncertainties for the slowest rates. Uncertainty for specific heat capacity is mainly determined by the uncertainty of the sample mass determination. It is in the order of ±10%, which is not perfect but allows for a comparison between different samples. Reproducibility of the obtained data for one sample measured under the same conditions and at the same rate is about ±2%. The good reproducibility of the heat capacity data allows a sensitive comparison of curves obtained after different thermal treatments. Next, an example of measurements on a polymer sample is presented.

4. Crystallization of polyethylene (PE)

The influence of cooling rate on the crystallization temperature of PE was studied in a wide range of scanning rates. The polymer sample commonly creates a good thermal contact with the membrane surface. But in order to improve the temperature distribution and to allow an easy replacement of the sample a gold foil (gold leave ca. 100 nm thick) was placed under the sample. In some cases the foil also helps to avoid spreading of the sample into the cold region of the membrane. In this particular case it was used to create similar experimental conditions in three different calorimeters. In case the sample–substrate interface acts as a nucleation site it should not be too different. In DSC experiments, thought to extend cooling rate range to lower rates, we use aluminum pans as sample container. To make the substrate for the fast scanning experiments also metallic the 100 nm thick gold foil was used (Fig. 9(a)).

Ultra high molecular weight polyethylene (UHMWPE) was chosen as a model system because of its stability, very high crys-

tallization rate and a large number of existing studies, e.g. [33]. The resulting heat capacity curves from cooling and heating scans at different rates are shown in Fig. 9(b). The sample mass was ca. 5 ng which is not big enough to give a good signal at low scanning rates. 500 K/s is the slowest rate with a reliable signal. But the low sample mass increases the highest possible rate. Crystallization and melting were observed in the scanning rate range of 100–10,000 K/s. Except the curves at 100 K/s heat capacity is reproducible within ±2%. As shown in Fig. 9(b) with increasing cooling rate the crystallization peak shifts to lower temperatures. Covering such wide range in cooling rates makes peak position meaningless because even a thermal lag of 1 ms creates a serious shift for a peak with a magnitude of about 5 times that of the baseline heat capacity. The shift for the peak may be about 50 K at 10,000 K/s compared to 5 K for the onset according the data shown in Ref. [17]. Therefore the rate dependence of crystallization peak onset temperature is shown in Fig. 9(c).

Because nonisothermal crystallization kinetics in a wider range of scanning rates was of interest two other calorimeters were used too. A Mettler Toledo DSC 822 was measuring an 11 mg sample at slow rates down to 1 mK/s and a PerkinElmer Pyris 1 DSC was measuring a ca. 1 mg sample from 0.05 to 2 K/s. There is still a gap of two orders of magnitude in scanning rate between the PerkinElmer DSC and the Fast Scanning setup. But the general tendency of the peak onset reveals a relatively smooth line covering 7 orders of magnitude in scanning rate. Even the fastest rates of 1 MK/s [14] are not possible with the device and the sensor used, the benefits of the new power compensation differential scanning nano-calorimeter are feasible. The ability to perform fast controlled temperature treatments at the same sample and the advanced heat capacity determination makes it a versatile device for routine investigations of polymers [23–25] and metals [17,27,28,34].

5. Summary

In the first part of this paper [17] we describe a new differential power compensated fast scanning calorimeter on the basis of thin film chip sensors. Depending on sample, size, and shape heating and cooling at controlled rates between 1 and 100,000 K/s is possible. Besides the big advantages regarding fast scanning the used thin film chip sensors must be considered as two-dimensional calorimeters. All problems known from two-dimensional DSCs [22] apply also to these calorimeters. There are heat flows to the surrounding not recognized by the measuring system, which cannot be corrected for by a measurement of an empty sensor as in conventional DSCs because they depend on the sample itself.

In this part of the paper we describe a procedure to obtain reliable heat capacity data even under non-ideal experimental conditions. For polymer samples of a few 10 ng heat capacity can be obtained with an uncertainty of about ±10% and reproducibility at optimum measurement conditions is about ±2%. At slow rates, when signal to noise ratio becomes bad or at high rates when the device reaches its limit, the uncertainty becomes larger and limits the applicability of the device. Reliable temperature measurements with an uncertainty of ±4 K are possible if a tiny indium or other reference material sample is placed on top of the polymer sample.

The device was applied to the study of crystallization and melting of UHMWPE. In combination with two other conventional DSCs a scanning rate range of 7 orders of magnitude was covered. Including data from single sensor fast scanning calorimetry [14] the dynamic range is extended by two more decades covering 9 orders of magnitude in total [35]. Furthermore scanning rates down to 1 μK/s are feasible [36], allowing calorimetric experiments in a very limited temperature range, because of time limitations, covering 12 orders of magnitude in scanning rate.

Acknowledgements

We acknowledge helpful discussions with Alexander Minakov, Dongshan Zhou, Wenbing Hu and YuLai Gao as well as financial support by a European Union funded Marie Curie EST fellowship (EZ), Humboldt-Foundation, Bosch-Foundation and Functional Materials Rostock e.V. (commercial supplier of AC and fast scanning chip calorimeters).

References

[1] M.F.J. Pijpers, V.B.F. Mathot, B. Goderis, R. Scherrenberg, E. van der Vegte, High-speed calorimetry for the analysis of kinetics of vitrification, crystallization and melting of macromolecule, Macromolecules 35 (2002) 3601–3613.
[2] H. Janeschitz-Kriegl, Crystallization Modalities in Polymer Melt Processing, Fundamental Aspects of Structure Formation, Springer, Wien, New York, 2010.
[3] V. Brucato, S. Piccarolo, V. La Carrubba, An experimental methodology to study polymer crystallization under processing conditions. The influence of high cooling rates, Chem. Eng. Sci. 57 (2002) 4129–4143.
[4] PerkinElmer_Inc., Technical Specifications Thermal Analysis for the DSC 8000/8500 Differential Scanning Calorimeters, http://las.perkinelmer.com/content/RelatedMaterials/SpecificationSheets/SPC_8000and8500.pdf, 2009.
[5] N.E. Hager, Thin heater calorimeter, Rev. Sci. Instrum. 35 (1964) 618–624.
[6] L.H. Allen, G. Ramanath, S.L. Lai, Z. Ma, S. Lee, D.D.J. Allman, K.P. Fuchs, 1000 000 °C/S thin film electrical heater: In situ resistivity measurements of Al and Ti/Si thin films during ultra rapid thermal annealing, Appl. Phys. Lett. 64 (1994) 417–419.
[7] M.Y. Efremov, E.A. Olson, M. Zhang, F. Schiettekatte, Z. Zhang, L.H. Allen, Ultrasensitive, fast, thin-film differential scanning calorimeter, Rev. Sci. Instrum. 75 (2004) 179–191.
[8] A.F. Lopeandia, E. Leon-Gutierrez, J. Rodriguez-Viejo, F.J. Munoz, Design issues involved in the development of a membrane-based high-temperature nanocalorimeter, Microelectron. Eng. 84 (2007) 1288–1291.
[9] R. Karmouch, J.F. Mercure, F. Schiettekatte, Nanocalorimeter fabrication procedure and data analysis for investigations on implantation damage annealing, Thermochim. Acta 432 (2005) 186–191.
[10] A.F. Lopeandia, J. Rodriguez-Viejo, M. Chacon, M.T. Clavaguera-Mora, F.J. Munoz, Heat transfer in symmetric U-shaped microreactors for thin film calorimetry, J. Micromech. Microeng. 16 (2006) 965–971.
[11] M.Y. Efremov, E.A. Olson, M. Zhang, S.L. Lai, F. Schiettekatte, Z.S. Zhang, L.H. Allen, Thin-film differential scanning nanocalorimetry: heat capacity analysis, Thermochim. Acta 412 (2004) 13–23.
[12] E.A. Olson, M.Y. Efremov, M. Zhang, Z.S. Zhang, L.H. Allen, The design and operation of a MEMS differential scanning nanocalorimeter for high-speed heat capacity measurements of ultrathin films, J. Microelectromech. Syst. 12 (2003) 355–364.
[13] A.A. Minakov, A.W. van Herwaarden, W. Wien, A. Wurm, C. Schick, Advanced nonadiabatic ultrafast nanocalorimetry and superheating phenomenon in linear polymers, Thermochim. Acta 461 (2007) 96–106.
[14] A.A. Minakov, C. Schick, Ultrafast thermal processing and nanocalorimetry at heating and cooling rates up to 1 MK/s, Rev. Sci. Instrum. 78 (2007) 073902–073910.
[15] A.A. Minakov, S.A. Adamovsky, C. Schick, Non adiabatic thin-film (chip) nanocalorimetry, Thermochim. Acta 432 (2005) 177–185.
[16] S.A. Adamovsky, A.A. Minakov, C. Schick, Scanning microcalorimetry at high cooling rate, Thermochim. Acta 403 (2003) 55–63.
[17] E. Zhuravlev, C. Schick, Fast Scanning Power Compensated Differential Scanning Nano-Calorimeter: 1. The Device, Thermochim. Acta 505 (2010) 1–13.
[18] A.W. van Herwaarden, Overview of calorimeter chips for various applications, Thermochim. Acta 432 (2005) 192–201.
[19] A. Minakov, J. Morikawa, T. Hashimoto, H. Huth, C. Schick, Temperature distribution in a thin-film chip utilized for advanced nanocalorimetry, Meas. Sci. Technol. 17 (2006) 199–207.
[20] A.F. Lopeandia, L.l. Cerdo, M.T. Clavaguera-Mora, L.R. Arana, K.F. Jensen, F.J. Munoz, J. Rodriguez-Viejo, Sensitive power compensated scanning calorimeter for analysis of phase transformations in small samples, Rev. Sci. Instrum. 76 (2005) 065104–065105.
[21] E. Zhuravlev, C. Schick, Patent pending (2009).
[22] C. Schick, Differential scanning calorimetry (DSC) of semicrystalline polymers, Anal. Bioanal. Chem. 395 (2009) 1589–1611.
[23] S. Guns, P. Kayaert, J.A. Martens, V.H. Jan, V. Mathot, T. Pijpers, E. Zhuravlev, C. Schick, V.d.M. Guy, Characterization of the copolymer poly(ethyleneglycol-g-vinylalcohol) as a potential carrier in the formulation of solid dispersions, Eur. J. Pharm. Biopharm. 74 (2010) 239–247.
[24] D. Mileva, R. Androsch, E. Zhuravlev, C. Schick, Critical rate of cooling for suppression of crystallization in random copolymers of propylene with ethylene and 1-butene, Thermochim. Acta 492 (2009) 67–72.
[25] D. Mileva, R. Androsch, E. Zhuravlev, C. Schick, Temperature of melting of the mesophase of isotactic polypropylene, Macromolecules 42 (2009) 7275–7278.
[26] Y. Gao, C. Zou, B. Yang, Q. Zhai, J. Liu, E. Zhuravlev, C. Schick, Nanoparticles of SnAgCu lead-free solder alloy with an equivalent melting temperature of SnPb solder alloy, J. Alloys Compd. 484 (2009) 777–781.

[27] Y.L. Gao, E. Zhuravlev, C.D. Zou, B. Yang, Q.J. Zhai, C. Schick, Calorimetric measurements of undercooling in single micron sized SnAgCu particles in a wide range of cooling rates, Thermochim. Acta 482 (2009) 1–7.
[28] B. Yang, Y.L. Gao, C.D. Zou, Q.J. Zhai, E. Zhuravlev, C. Schick, Repeated nucleation in an undercooled tin droplet by fast scanning calorimetry, Mater. Lett. 63 (2009) 2476–2478.
[29] E.S. Watson, M.J. O'Neill, Differential Micro Calorimeter, US patent 3,263,484 (1962).
[30] W. Hemminger, G.W.H. Hohne, Calorimetry—Fundamentals and Practice, Vch, Weinheim, 1984.
[31] B. Wunderlich, The athas database on heat capacities of polymers, Pure Appl. Chem. 67 (1995) 1019–1026, see on WWW URL: http://athas.prz.edu.pl/Default.aspx?op=db.
[32] B. Wunderlich, Precision heat capacity measurements for the characterization of two-phase polymers, J. Therm. Anal. 30 (1985) 1217–1221.
[33] S. Rastogi, Y. Yao, D.R. Lippits, G.W.H. Höhne, R. Graf, H.W. Spiess, P.J. Lemstra, Segmental mobility in the non-crystalline regions of semicrystalline polymers and its implications on melting, Macromol. Rapid Commun. 30 (2009) 826–839.
[34] G. YuLai, Z. ChangDong, Y. Bin, Z. QiJie, Fast calorimetric scanning of micro-sized SnAgCu single droplet at a high cooling rate, Sci. China Ser E-Tech. Sci. 52 (2009) 1707–1711.
[35] R. Androsch, M.L. Di Lorenzo, C. Schick, B. Wunderlich, Mesophases in polyethylene, polypropylene and poly(1-butene), Polymer (submitted for publication).
[36] S. Wang, K. Tozaki, H. Hayashi, S. Hosaka, H. Inaba, Observation of multiple phase transitions in n-C22H46 using a high resolution and super-sensitive DSC, Thermochim. Acta 408 (2003) 31–38.